J. Fluid Mech. (1986), *vol.* 162, *pp.* 415–438
Printed in Great Britain

On the fine structure of osmosis including three-dimensional pore entrance and exit behaviour

By ZONG-YI YAN†, SHELDON WEINBAUM
Department of Mechanical Engineering, The City College of the City University of New York, New York, NY 10031

AND ROBERT PFEFFER
Department of Chemical Engineering, The City College of The City University of New York, New York, NY 10031

(Received 29 January 1985 and in revised form 2 July 1985)

This paper presents a detailed quantitative model of osmotic fine structure for both permeable and semi-permeable membranes in dilute bathing solutions. The analysis differs from all previous studies in that it treats for the first time, albeit in an approximate manner, the detailed three-dimensional hydrodynamic interaction of the particles in the entrance and exit regions and the coupling of the convective–diffusive effects in these regions with those in the interior of the pore. Reasonable interpolations between various asymptotic formulas are used to derive the tensorial components of the particle diffusivity and the slip between the fluid and particle phases as functions of position throughout the entire flow field. The solutions show that the entrance and exit regions in the case of permeable membranes can have a significant effect on the osmotic solvent flux q for small particles in short pores although changes in the overall reflection coefficient are small. This is due to the nonlinear sweeping effect of convection at the higher osmotic-flow rates. For semi-permeable membranes the predictions of the model support the hypothesis of Mauro (1957) and Ray (1960) that there is a region of near-discontinuity in pressure and concentration at the plane of the pore entrance and the sweeping effects of convection on the concentration profile are very minor for the dilute solutions studied herein. In contrast, the solutions for the permeable membrane clearly show the existence of three-dimensional unstirred regions which extend two-to-three pore radii from the pore openings. These solutions form the substructure of the much thicker one-dimensional unstirred layer described by Dainty (1963) and Pedley *et al.* (1978). It is shown that when the porosity is low (such as in most biological membranes), the wall concentration in Pedley's solution is the far-field concentration for the entrance/exit solutions presented herein.

1. Introduction

Osmotic phenomena are of great biological significance. Osmosis occurs across the plasmalemma membranes of all living cells and through the intercellular clefts of the epithelial and endothelial cell layers lining all the internal body organs such as the kidney tubules, blood capillaries, intestines, gall bladder and cornea. Other biological examples are the synthetic membranes in artificial organs and the water exchange in plant cells and tissues.

† Current address: Institute of Mechanics, Chinese Academy of Sciences, Beijing, China.

Osmotic flows have classically been treated either from the standpoint of irreversible thermodynamics or using detailed microhydrodynamic theories. In the thermodynamic approach the solute flow J_s and the total volume flux J_v are related to the difference of hydrodynamic and osmotic pressures, Δp and $\Delta\pi$, across the membrane, by the Kedem & Katchalsky (1958) equations:

$$J_s = \omega\Delta\pi + (1-\sigma)\bar{C}J_v, \tag{1a}$$

$$J_v = L_p(\Delta p - \sigma\Delta\pi), \tag{1b}$$

where L_p is the hydraulic permeability describing the viscous losses of the pure solvent in passing through the pore, σ is the reflection coefficient describing the hydrodynamic interaction of the solute particles with the pore walls including the entrance and the exit, ω is the diffusive permeability and $\bar{C}$ is some average concentration for the membrane. For a semi-permeable membrane where the particle radius is larger than the pore radius, $\sigma = 1$. The osmotic pressure for a dilute solution is given by van't Hoff's law (e.g. see Hsieh 1975):

$$\pi = \bar{R}TC, \tag{2}$$

where $\bar{R}$ is the universal gas constant and T the absolute temperature.

The Kedem–Katchalsky equations, while showing the equivalence of a transmembrane pressure difference and osmotic concentration difference, tell nothing about the detailed structure of the p- and C-profiles and thus whether the movement of the solvent is due to bulk flow or diffusion. Mauro (1957) and Ray (1960) have hypothesized that for a semi-permeable membrane there is a region of very steep concentration gradient at the entrance to the pore, of thickness about the same as the pore radius, and that the water in this region should diffuse much more rapidly than would occur because of a concentration gradient across the pores themselves. If this were the case the diffusional gradient due to the concentration difference at the entrance to the pore would establish a passive bulk flow of the solvent through the pore in which the pressure drop along the pore length is just equal to the osmotic-pressure difference at the pore entrance. No detailed model has ever been developed to prove this hypothesis since this theory would require a detailed analysis of the hydrodynamic interaction of the particles with the entrance geometry of the pore and a solution for the three-dimensional concentration field at the pore entrance. This same difficulty, of course, applies for permeable membranes, except that one now must also account for the hydrodynamic interaction of the particles with the walls of the pore and the coupling of the three-dimensional entrance and exit concentration and pressure fields with the solutions for these fields in the pore interior. To simplify this problem for permeable membranes, all previous investigators have neglected the pore entrance and exit effects and have developed various microhydrodynamic theories in which idealized models of the particle motion within a single pore have been considered (Anderson & Malone 1974; Anderson & Quinn 1974; Levitt 1975; Ganatos *et al.* 1980; Anderson 1981).

As Dainty (1963) and Pedley (1980, 1981) pointed out, near the plane of the membrane there is an 'unstirred layer' in which the solute concentration adjusts from C_m at the membrane plane to C_b in the bulk solution. Pedley & Fischbarg (1978) have proposed a one-dimensional analysis for the unstirred layer adjacent to a semi-permeable membrane in which the layer thickness is taken as known from measurements. Their results show that, under some circumstances, the neglect of the unstirred layer may incur significant error in estimating the osmotic flow. However,

as will be shown in this paper, for a permeable membrane the concentration field near the entrance or exit of the pore exhibits a clearly three-dimensional behaviour with a fine-scale substructure where Pedley's one-dimensional model cannot be applied. The present paper will provide important new insights into this substructure and into its relationship to Pedley's unstirred layer.

The present paper is a major departure from the earlier microhydrodynamic analyses in that it attempts to treat in an approximate manner the spatially varying three-dimensional hydrodynamic interaction of a spherical particle with the entrance and exit geometry of the pore and the consequence of this interaction on the detailed pressure and concentration profiles and the osmotic flux. Although the authors have just obtained the first accurate numerical solutions for the various force and torque coefficients for the three-dimensional particle–pore-entrance interaction (Yan *et al.* 1985), these solutions were not available before the present study was completed. Plausible interpolations between various asymptotic approximations have to be employed herein as well as other simplifying assumptions for these coefficients. The validity of these assumptions has now been confirmed by the numerical solutions in Yan *et al.* (1985). The approximate solutions for the force and torque coefficients are then used to determine the velocity of a neutrally buoyant particle in the absence of diffusive fluxes as well as the diffusivity tensor of the solute particle. Finally, the solute conservation equation is solved throughout the entire flow by matching separate solutions for the entrance and exit regions and the pore interior. Results will be presented for a wide range of particle-to-pore-radii ratios, pore-length-to-diameter ratios and particle concentrations within the dilute range. The upper limit on solute volume fraction ϕ has been arbitrarily chosen as 0.05. While this value of ϕ, at first glance, might seem large, since it entails a roughly 20 % error in osmotic pressure for hard spheres and 13 % error in the viscosity of the bulk solution, these errors are still an order of magnitude smaller than the entrance and exit effects for short pores and small particles.

The mathematical formulation, numerical procedure and results are presented in §§2, 3 and 4 respectively.

2. Formulation

We consider a membrane with a single circular pore of length l and radius R_0 (figure 1). The membrane separates two dilute solutions of different concentrations, C_∞ and $C_{-\infty}$. The solute particle's radius a can be either smaller (for a permeable membrane, figure 1*a*) or larger (for a semi-permeable membrane, figure 1*b*) than R_0. The solution is assumed to be so dilute that the hydrodynamic interactions between the particles are negligible. The broken lines in figures 1 (*a*) and (*b*) define the limiting positions at which the particle centres can be closest to the wall. Between these lines and the wall are the exclusion layers where no solute is present. Far from the pore openings the fluid pressures on the two sides of the membrane are assumed to be the same, i.e. $p_\infty = p_{-\infty}$.

2.1. *The constitutive equation of binary diffusion*

As Brenner & Gaydos (1977) pointed out, in the presence of hydrodynamic interaction the diffusive flux should be measured with respect not to the mass average velocity, but with respect to the deterministic velocity $\boldsymbol{U}^0$ of a neutrally buoyant particle:

$$\boldsymbol{U} = \boldsymbol{U}^0 - \boldsymbol{D}\cdot\frac{1}{C}\boldsymbol{\nabla}C. \tag{3}$$

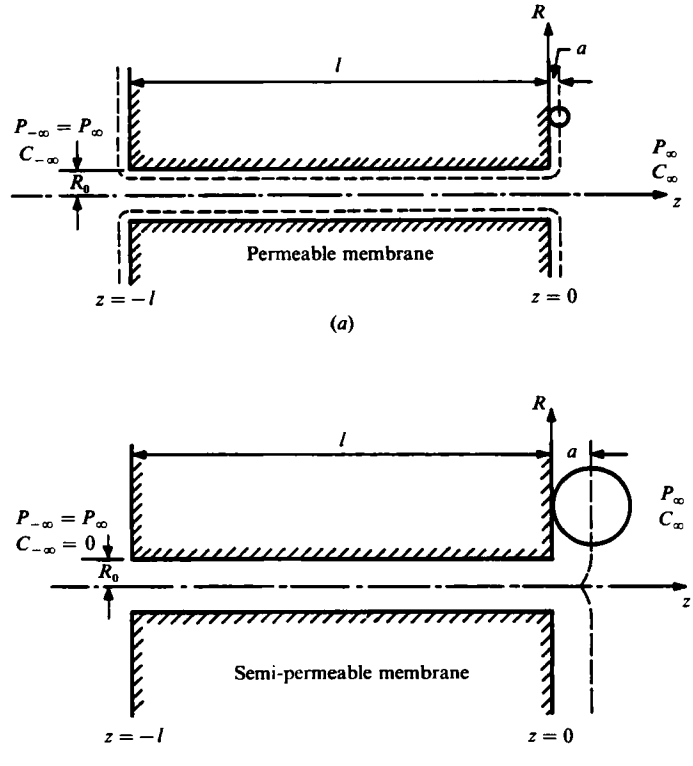

FIGURE 1. Our models for the fine structure of osmosis: (*a*) the permeable membrane; (*b*) the semi-permeable membrane.

To obtain the expressions for $\boldsymbol{U}^0$ and $\boldsymbol{D}$, we consider the force and torque balance for each osmotic particle. The thermodynamic force due to the Brownian diffusion (Batchelor 1976) is set equal to the total hydrodynamic force and the net torque set equal to zero. Since the total hydrodynamic force can be viewed as the superposition of a pure translation $\boldsymbol{U}$ and a pure rotation $\boldsymbol{\Omega}$ in a quiescent fluid, plus the flow $\boldsymbol{V}$ through the pore past a stationary particle, this momentum balance in the limit of low Re can be written approximately as

$$6\pi\mu a(U_R F_R^t + a\Omega F_R^r + V_R F_R^s) = \frac{1}{N_A}\frac{\bar{R}T}{C}\frac{\partial C}{\partial R}, \tag{4a}$$

$$6\pi\mu a(U_z F_z^t + a\Omega F_z^r + V_z F_z^s) = \frac{1}{N_A}\frac{\bar{R}T}{C}\frac{\partial C}{\partial z}, \tag{4b}$$

$$8\pi\mu a^2\left(U_R T_\phi^{t,R} + U_z T_\phi^{t,z} + a\Omega T_\phi^r + \frac{a}{2z} V_R T_\phi^{s,R} + \frac{a}{2R} V_z T_\phi^{s,z}\right) = 0, \tag{4c}$$

where N_A is Avogadro's number and the F_R^t, $T_\phi^{t,R}$, etc. are the hydrodynamic force and torque correction factors for each of the three motions mentioned above. The subscripts denote the direction of the force or torque and the superscripts the mode of motion including component direction. Equations (4*a*, *b*, *c*) involve two important simplifications. First, these equations neglect the fact that a translation in the R-direction can induce a force in the z-direction and *vice versa*. For motion near

an infinite plane wall these orthogonal forces vanish for a hard sphere: however, this is not true in the presence of a pore opening where the motion of particle generates a flux through the pore. Secondly, the torque correction factors $T_\phi^{s,R}$ and $T_\phi^{s,z}$ are not independent. Both these simplifications have since been justified by the more rigorous numerical solutions in Yan *et al.* (1985).

Solving (4*c*) for $\boldsymbol{\Omega}$ and rewriting (4*a*, *b*) in vector form, we have

$$\boldsymbol{U}\cdot\boldsymbol{\lambda}^{(U)}+\boldsymbol{V}\cdot\boldsymbol{\lambda}^{(V)}=\frac{\bar{R}T}{6\pi\mu a N_A}\frac{1}{C}\nabla C, \tag{5}$$

where $\boldsymbol{\lambda}^{(U)}$ and $\boldsymbol{\lambda}^{(V)}$ are friction tensors for the particle motion $\boldsymbol{U}$ and the fluid motion $\boldsymbol{V}$ and their components are given by

$$\left.\begin{aligned}
\lambda_{RR}^{(U)} &= F_R^t-\frac{F_R^r T_\phi^{t,R}}{T_\phi^r}, & \lambda_{RR}^{(V)} &= F_R^s-\frac{(a/2z)\,F_R^r T_\phi^{s,R}}{T_\phi^r},\\
\lambda_{Rz}^{(U)} &= -\frac{F_R^r T_\phi^{t,z}}{T_\phi^r}, & \lambda_{Rz}^{(V)} &= -\frac{(a/2R)\,F_R^r T_\phi^{s,z}}{T_\phi^r},\\
\lambda_{zR}^{(U)} &= -\frac{F_z^r T_\phi^{t,R}}{T_\phi^r}, & \lambda_{zR}^{(V)} &= -\frac{(a/2z)\,F_z^r T_\phi^{s,R}}{T_\phi^r},\\
\lambda_{zz}^{(U)} &= F_z^t-\frac{F_z^r T_\phi^{t,z}}{T_\phi^r}, & \lambda_{zz}^{(V)} &= F_z^s-\frac{(a/2R)\,F_z^r T_\phi^{s,z}}{T_\phi^r}.
\end{aligned}\right\} \tag{6}$$

The relation between $\boldsymbol{U}^0$ and $\boldsymbol{V}$ for a neutrally buoyant particle can be found by setting the thermodynamic force in (5) equal to zero:

$$\left.\begin{aligned}
U_R^0 &= -\frac{1}{\lambda^{(U)}}\left[(\lambda_{RR}^{(V)}\lambda_{zz}^{(U)}-\lambda_{zR}^{(V)}\lambda_{Rz}^{(U)})\,V_R+(\lambda_{Rz}^{(V)}\lambda_{zz}^{(U)}-\lambda_{zz}^{(V)}\lambda_{Rz}^{(U)})\,V_z\right],\\
U_z^0 &= -\frac{1}{\lambda^{(U)}}\left[(\lambda_{Rz}^{(V)}\lambda_{RR}^{(U)}-\lambda_{RR}^{(V)}\lambda_{zR}^{(U)})\,V_R+(\lambda_{zz}^{(V)}\lambda_{RR}^{(U)}-\lambda_{Rz}^{(V)}\lambda_{zR}^{(U)})\,V_z\right],
\end{aligned}\right\} \tag{7}$$

where

$$\lambda^{(U)}=\lambda_{RR}^{(U)}\lambda_{zz}^{(U)}-\lambda_{Rz}^{(U)}\lambda_{zR}^{(U)}.$$

The expressions for the diffusivity tensor are similarly obtained by solving the force-balance equation (5) when $\boldsymbol{V}=\boldsymbol{U}^0=0$ and comparing the results with the definition of $\boldsymbol{D}$ in (3):

$$\left.\begin{aligned}
D_{RR} &= D_\infty\left(\frac{-\lambda_{zz}^{(U)}}{\lambda^{(U)}}\right), & D_{Rz} &= D_\infty\left(\frac{\lambda_{zz}^{(U)}}{\lambda^{(U)}}\right),\\
D_{zR} &= D_\infty\left(\frac{\lambda_{zR}^{(U)}}{\lambda^{(U)}}\right), & D_{zz} &= D_\infty\left(\frac{-\lambda_{RR}^{(U)}}{\lambda^{(U)}}\right),
\end{aligned}\right\} \tag{8a}$$

where

$$D_\infty=\frac{\bar{R}T}{6\pi\mu a N_A} \tag{8b}$$

is the diffusivity of a spherical solute particle in an unbounded medium.

2.2. *Solution for a permeable membrane*

From (3) the solute conservation equation is given by

$$\nabla\cdot(C\boldsymbol{U}^0)=\nabla\cdot(\boldsymbol{D}\cdot\nabla C). \tag{9}$$

For a permeable membrane as shown in figure 1 (*a*), (9) is solved separately for the regions inside and outside the pore. However, for the flow inside the pore, there is

at present no theory for determining the hydrodynamic coefficients that would appear in the expression for U_R^0 or D_{RR}. Fortunately, for most membranes of practical interest the pore length l is much larger than the pore radius R_0 and, thus, we can reasonably use the one-dimensional approximation to equation (9), with U_z^0 and C as constants over the cross-section:

$$\frac{\mathrm{d}}{\mathrm{d}z}(CU_z^0) = \frac{\mathrm{d}}{\mathrm{d}z}\left(D_{zz}\frac{\mathrm{d}C}{\mathrm{d}z}\right), \tag{10}$$

where

$$U_z^0 = -\frac{F_{z0}^s}{F_{z0}^t}\bar{V}_z, \quad D_{zz} = D_\infty\left(\frac{-1}{F_{z0}^t}\right), \tag{11a, b}$$

and $\bar{V}_z$ is the average velocity of the solvent in the pore; F_{z0}^t and F_{z0}^s should be the hydrodynamic coefficients averaged over the pore cross-section but are approximated by their values at the centreline. U_z^0 and D_{zz} can be taken as constants throughout the pore interior. The solution to (10) which satisfies the unknown concentrations $C(0) = C_0$ and $C(-l) = C_l$ at the entrance and exit planes is

$$C(z) = \frac{(C_0 - C_l)\,\mathrm{e}^{U_z^0 z/D_{zz}} + C_l - C_0\,\mathrm{e}^{-U_z^0 l/D_{zz}}}{1 - \mathrm{e}^{-U_z^0 l/D_{zz}}} \quad (-l \leqslant z \leqslant 0). \tag{12}$$

To find the relationship between the concentration and pressure profiles, we use the differential form of the Kedem–Katchalsky equation (1b):

$$J_\mathrm{v} = \Lambda_p\left(\frac{\mathrm{d}p}{\mathrm{d}z} - \sigma\bar{R}T\frac{\mathrm{d}C}{\mathrm{d}z}\right), \tag{13}$$

where Λ_p is the local hydraulic permeability in place of the overall coefficient L_p. With the porosity η of the membrane defined as the ratio of the pore cross-section to membrane area, the Poiseuille formula leads to

$$\Lambda_p = \left(\frac{J_\mathrm{v}}{\mathrm{d}p/\mathrm{d}z}\right)_{\mathrm{d}C/\mathrm{d}z\,=\,0} = \frac{\eta R_0^2}{8\mu}. \tag{14}$$

The reflection coefficient inside a circular cylindrical pore, where the value of σ is denoted by σ_0, has been given by Anderson & Adamski (1983):

$$\sigma = \sigma_0 = \tilde{a}^2(4 - 4\tilde{a} + \tilde{a}^2) + \tfrac{4}{3}\tilde{a}^2(1 - \tilde{a})^2, \tag{15a}$$

where

$$\tilde{a} = \frac{a}{R_0}. \tag{15b}$$

In terms of the volumetric flow rate, defined as

$$q = \bar{V}_z \pi R_0^2, \tag{16}$$

(13) can be written as

$$\frac{\mathrm{d}p}{\mathrm{d}z} = \sigma_0\bar{R}T\frac{\mathrm{d}C}{\mathrm{d}z} - \frac{8\mu q}{\pi R_0^4}. \tag{17}$$

The integration of (17) gives

$$p(z) - p(0) = \sigma_0\bar{R}T(C(z) - C_0) - \frac{8\mu q}{\pi R_0^4}z \quad (-l \leqslant z \leqslant 0). \tag{18}$$

The total pressure drop along the pore is

$$p(-l) - p(0) = \sigma_0\bar{R}T(C_l - C_0) + \frac{8\mu q l}{\pi R_0^4}. \tag{19}$$

Outside the pore, in the entrance and exit regions, we shall solve the three-dimensional version of (9) for axisymmetric convection and diffusion:

$$\frac{1}{R}\frac{\partial}{\partial R}(CU_R^0 R)+\frac{\partial}{\partial z}(CU_z^0)=\frac{1}{R}\frac{\partial}{\partial R}\left(D_{RR}R\frac{\partial C}{\partial R}+D_{Rz}R\frac{\partial C}{\partial z}\right)+\frac{\partial}{\partial z}\left(D_{zR}\frac{\partial C}{\partial R}+D_{zz}\frac{\partial C}{\partial z}\right). \tag{20a}$$

To find $\boldsymbol{U}^0$ and $\boldsymbol{D}$ one must first evaluate all the force and torque coefficients in (6) for $\boldsymbol{\lambda}^{(U)}$ and $\boldsymbol{\lambda}^{(V)}$ as functions of particle position. The approximations for these coefficients are summarized in §2.4. The boundary conditions in the right half-space ($z>0$) (see figure 1*a*) are:

$$C=C_\infty, \quad \text{when } (R^2+z^2)^{\frac{1}{2}}\to\infty \text{ and } z>a; \tag{20b}$$

$$\frac{\partial C}{\partial R}=0, \quad \text{when } R=0; \tag{20c}$$

$$CU_z=CU_z^0-D_{zR}\frac{\partial C}{\partial R}-D_{zz}\frac{\partial C}{\partial z}=0, \quad \text{when } z=a \text{ and } R\geqslant R_0 \text{ or } z=(a^2-(R_0-R)^2)^{\frac{1}{2}} \text{ and } R_0-a\leqslant R<R_0; \tag{20d}$$

$$C_{z=0^+}=C_{z=0^-}, \quad \text{when } z=0 \text{ and } R<R_0-a; \tag{20e}$$

$$\left(\frac{\partial C}{\partial z}\right)_{z=0^+}=\left(\frac{\mathrm{d}C}{\mathrm{d}z}\right)_{z=0^-}, \quad \text{when } z=0 \text{ and } R<R_0-a. \tag{20f}$$

An equivalent set of boundary conditions apply in the left half-space ($z<-l$). The matching conditions for concentration gradient $(\mathrm{d}C/\mathrm{d}z)_{z=0^-}$ and $(\mathrm{d}C/\mathrm{d}z)_{z=-l^+}$ are evaluated from the concentration profile (12) inside the pore:

$$\left(\frac{\mathrm{d}C}{\mathrm{d}z}\right)_{z=0^-}=\frac{U_z^0(C_0-C_l)}{D_{zz}(1-\mathrm{e}^{-U_z^0 l/D_{zz}})},$$

$$\left(\frac{\mathrm{d}C}{\mathrm{d}z}\right)_{z=-l^+}=\left(\frac{\mathrm{d}C}{\mathrm{d}z}\right)_{z=0^-}\mathrm{e}^{-U_z^0 l/D_{zz}}.$$

In (5) $\boldsymbol{V}$ is the solvent velocity. When the solution is dilute, it should differ very little from that of a pure-solvent flow. The exact solution of Dagan, Weinbaum & Pfeffer (1982*a*) shows that this velocity can be closely approximated by the Poiseuille profile inside the pore or Sampson's solution outside the pore. In the right half-space Sampson's solution can be written as (see Happel & Brenner 1973, p. 193)

$$V_R=\frac{3q}{8\pi R_0^2}z\frac{\zeta}{R}(R_2-R_1)\left(\frac{1}{R_1}-\frac{1}{R_2}\right), \tag{21a}$$

$$V_z=\frac{3q}{8\pi R_0^2}\frac{\zeta}{R}(R_1-R_2)\left(\frac{R-R_0}{R_1}-\frac{R+R_0}{R_2}\right), \tag{21b}$$

where q is the volumetric flow rate of the solvent through the pore,

$$\zeta=\left(1-\frac{(R_1-R_2)^2}{4R_0^2}\right)^{\frac{1}{2}}, \tag{21c}$$

and

$$R_1=(z^2+(R-R_0)^2)^{\frac{1}{2}}, \quad R_2=(z^2+(R+R_0)^2)^{\frac{1}{2}}. \tag{21d}$$

To find the pressure variation, we apply the differential form of the Kedem–Katchalsky equations (1*a*) and (1*b*) along the centreline ($R = 0$). The differential form of (1*a*) is

$$J_s = \omega'(z)\,\bar{R}T\frac{\partial C}{\partial z} + (1-\sigma(z))\,CJ_v, \tag{22a}$$

Here $\omega'(z)$ and $\sigma(z)$ are the local diffusive permeability and the local reflection coefficient respectively and C is the concentration that would exist for local thermodynamic equilibrium. This equation can be rewritten as

$$\eta C U_z = \omega'(z)\,\bar{R}T\frac{\partial C}{\partial z} + (1-\sigma(z))\,C\eta\,\bar{V}_z. \tag{22b}$$

Substituting (6), (7) and (8), with the hydrodynamic coefficients given in §2.4, into (3) and comparing this with (22*b*), we have

$$\sigma(z) = 1 + \left(\frac{F_z^s}{F_z^t}\right)_{R=0}. \tag{22c}$$

Note that, when z is large, $F_z^s/F_z^t \to -1$ and thus $\sigma(z) \to 0$. The small discrepancies between the results given by (15) and (22*c*) at the pore opening are handled by interpolation. Using the Sampson velocity profile (21*a*) and (21*b*), we have

$$p(z)-p(0) = \int_0^z \sigma(z)\,\bar{R}T\frac{\partial C}{\partial z}\,\mathrm{d}z - \frac{3\mu q}{\pi R_0^3}\left[\frac{zR_0}{R_0^2+z^2} + \tan^{-1}\left(\frac{z}{R_0}\right)\right] \quad (R=0,\, z>0), \tag{23}$$

and

$$p_\infty - p(0) = \int_0^\infty \sigma(z)\,\bar{R}T\frac{\partial C}{\partial z}\,\mathrm{d}z - \frac{3\mu q}{2R_0^3}. \tag{24}$$

Similarly, in the left half-space we have

$$p(z)-p(-l) = \int_{-l}^z \sigma(z)\,\bar{R}T\frac{\partial C}{\partial z}\,\mathrm{d}z - \frac{3\mu q}{\pi R_0^3}\left[\frac{(z+l)\,R_0}{(z+l)^2+R_0^2} + \tan^{-1}\left(\frac{z+l}{R_0}\right)\right] \quad (R=0,\, z<-l), \tag{25}$$

and

$$p_{-\infty} - p(-l) = \int_{-l}^{-\infty} \sigma(z)\,\bar{R}T\frac{\partial C}{\partial z}\,\mathrm{d}z + \frac{3\mu q}{2R_0^3}. \tag{26}$$

Combining (19), (24) and (26) and using $p_\infty = p_{-\infty}$, we can derive an expression for the osmotic-flow rate:

$$q = \frac{R_0^3}{\mu}\,\frac{\sigma_0\,\bar{R}T(C_0-C_l) + \int_0^\infty \sigma(z)\,\bar{R}T\frac{\partial C}{\partial z}\,\mathrm{d}z - \int_{-l}^{-\infty} \sigma(z)\,\bar{R}T\frac{\partial C}{\partial z}\,\mathrm{d}z}{3+\dfrac{8l}{\pi R_0}}. \tag{27}$$

The three terms in the numerator describe the contribution to the total flux of the osmotic forces in the interior and entrance/exit regions, whereas the denominator denotes the hydrodynamic resistance to the solvent movement outside and inside the pore.

2.3. *Solution for a semi-permeable membrane*

For a semi-permeable membrane where $R_0 < a$ (figure 1*b*), we solve the axisymmetric continuity equation (20*a*) in the right half-space ($z > 0$) subject to the following boundary conditions:

$$C = C_\infty \quad \text{when } (R^2+z^2)^{\frac{1}{2}} \to \infty \text{ and } z > a; \tag{28a}$$

$$\frac{\partial C}{\partial R} = 0 \quad \text{when } R = 0; \tag{28b}$$

$$CU_z = CU_z^0 - D_{zR}\frac{\partial C}{\partial R} - D_{zz}\frac{\partial C}{\partial z} = 0 \quad \text{when } z = a \text{ and } R \geqslant R_0$$

$$\text{or } z = (a^2-(R_0-R)^2)^{\frac{1}{2}} \text{ and } R < R_0. \tag{28c}$$

Because $R_0 < a$, the steric exclusion establishes an abrupt change in pressure as well as in concentration across the broken curve in figure 1(*b*). Along the centreline ($R = 0$), we have

$$p(z_a^+) - \bar{R}TC(z_a^+) = p(z_a^-) \quad (R = 0), \tag{29a}$$

where

$$z_a = (a^2 - R_0^2)^{\frac{1}{2}}. \tag{29b}$$

To the left of $z = z_a$, the concentration is identically zero and the pressure drop is due to Sampson's solution alone:

$$p(z) - p(0) = -\frac{3\mu q}{\pi R_0^3}\left[\frac{zR_0}{z^2+R_0^2} + \tan^{-1}\left(\frac{z}{R_0}\right)\right] \quad (R = 0,\ 0 < z < z_a). \tag{30}$$

The pressure to the right of $z = z_a$ can be evaluated in a way similar to (23). Combining these results, we obtain

$$p(z) - p(0) = \int_{z_a}^{z} \sigma(z)\,\bar{R}T\frac{\partial C}{\partial z}\,\mathrm{d}z + \bar{R}TC(z_a^+) - \frac{3\mu q}{\pi R_0^3}\left[\frac{zR_0}{z^2+R_0^2} + \tan^{-1}\left(\frac{z}{R_0}\right)\right]$$

$$(R = 0,\ z > z_a), \tag{31}$$

and

$$p_\infty - p(0) = \int_{z_a}^{\infty} \sigma(z)\,\bar{R}T\frac{\partial C}{\partial z}\,\mathrm{d}z + RTC(z_a^+) - \frac{3\mu q}{2R_0^3}. \tag{32}$$

The analogue to (27) is

$$q = \frac{R_0^3}{\mu}\,\frac{\bar{R}TC(z_a^+) + \int_{z_a}^{\infty} \sigma(z)\,\bar{R}T\dfrac{\partial C}{\partial z}\,\mathrm{d}z}{3 + \dfrac{8l}{\pi R_0}}. \tag{33}$$

2.4. *Consideration of hydrodynamic interactions*

Inside the pore, the data for F_{z0}^t and F_{z0}^s can be taken from Happel & Brenner (1973, p. 318) for small particles or from Leichtberg, Pfeffer & Weinbaum (1976) for large particles.

Outside the pore, the spatially varying hydrodynamic data for the force and torque correction factors appearing in (6) were not available when this study was first undertaken. However, we do know their asymptotic behaviours for the important limiting cases. The values of F_z^t and F_z^s for the axisymmetric flow when the sphere centre is located on the pore axis have been obtained by Dagan, Weinbaum & Pfeffer (1982*b*). When the sphere is far away from the pore opening, the pore effect becomes negligible so that the plane wall with a pore may conceptually be replaced by an infinite solid wall. The R-component of the flow past a fixed sphere near the plane of the pore wall is reasonably approximated by a linear shear flow past a sphere in the presence of an infinite wall. The coefficients for all the infinite-wall cases except F_z^s have been obtained by Brenner and co-workers: F_z^t is given in Brenner (1961), F_R^s and $T_\phi^{s,R}$ are found in Cox & Brenner (1967), F_R^t, $T_\phi^{t,R}$, F_R^τ and T_ϕ^τ are presented

z/a	F_R^t	F_R^r	F_R^s	T_ϕ^r	$T_\phi^{t,R}$	$T_\phi^{s,R}$
1.0000	∞	∞	1.7005	∞	∞	0.9440
1.0032	−4.0223	0.5133	1.6982	−2.6793	0.3849	0.9443
1.0050	−3.7863	0.4558	1.6969	−2.5056	0.3419	0.9444
1.0453	−2.6475	0.1840	1.6682	−1.6996	0.1455	0.9477
1.1276	−2.1514	9.829×10^{-2}	1.6160	−1.3877	7.372×10^{-2}	0.9537
1.5431	−1.5675	1.953×10^{-2}	1.4391	−1.0998	1.456×10^{-2}	0.9742
2.3524	−1.3079	3.523×10^{-3}	1.2780	−1.0250	2.642×10^{-3}	0.9901
3.7622	−1.1738	5.621×10^{-4}	1.1671	−1.0059	4.216×10^{-4}	0.9971
10.0677	−1.0591	1.170×10^{-5}	1.0587	−1.0003	8.774×10^{-6}	0.9981
∞	−1.0000	0.000	1.0000	−1.0000	0.000	1.0000

TABLE 1. Part of the force and torque correction factors

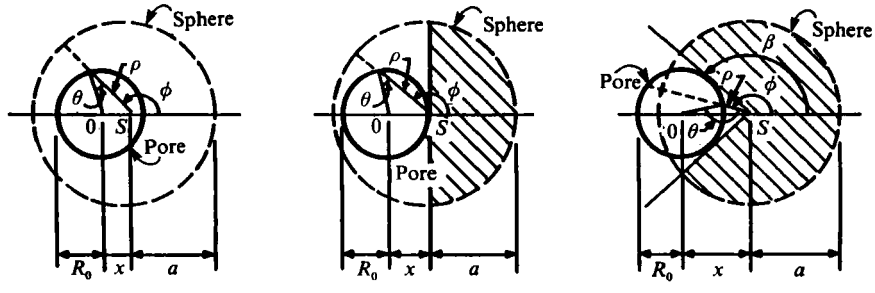

FIGURE 2. Three cases for the calculations of F_z^t and F_z^s.

in Goldman, Cox & Brenner (1967). The coefficient F_z^s is well approximated by the stagnation-point flow past a sphere in the presence of a large-but-finite disk (Dagan, Pfeffer & Weinbaum 1982), since the infinite-plane-wall solutions do not permit a finite flow normal to the plane of the membrane.

One anticipates that the presence of the pore opening will have the greatest influence on F_z^t and F_z^s since these motions involve a large flow through the pore opening. Significant departures of these coefficients from the infinite-wall cases can be expected and special treatment is required. In contrast, the rotation or translation of the sphere parallel to the wall induces a much smaller flow through the pore. These motions can, therefore, be reasonably approximated by an appropriate infinite-wall solution. In addition several of the coefficients are identically zero for the infinite plane wall and should be small compared with unity when the pore is present. In view of these observations we shall make the following assumptions:

(i) $F_z^r = T_\phi^{t,z} = T_\phi^{s,z} = 0$;

(ii) F_R^t, F_R^r, F_R^s, T_ϕ^r, $T_\phi^{t,R}$ and $T_\phi^{s,R}$ are relatively insensitive to the radial position R and, thus, can be approximated by the results for a sphere near an infinite solid wall as summarized in table 1;

(iii) F_z^t and F_z^s are interpolated using known solutions for the axisymmetric motion of a sphere near an orifice or disk (Dagan *et al.* 1982*b*; Dagan *et al.* 1982). The details of this interpolation are given in Yan (1985) and are summarized in figure 2. Three cases are identified in this figure, the projection S of the sphere centre lying (*a*) inside, (*b*) on the edge and (*c*) outside the pore. In case (*a*) the local radius ρ from S to the

z/R_0	$R/R_0 = 0$	0.25	0.50	0.75	1.00	1.50	2.00	5.00	∞
				$-F_z^t$					
0.50	1.3688	1.4335	1.6495	2.7967	∞	∞	∞	∞	∞
0.55	1.3777	1.4349	1.6271	2.4097	6.7243	10.0157	10.6767	11.3378	11.4592
0.75	1.3882	1.4310	1.5628	1.8157	2.3584	2.9414	3.0703	3.1838	3.2054
1.00	1.3919	1.4159	1.4949	1.5986	1.7609	2.0023	2.0686	2.1163	2.1255
2.00	1.3019	1.2956	1.3008	1.3064	1.3153	1.3478	1.3662	1.3787	1.3802
5.00	1.1240	1.1229	1.1226	1.1225	1.1225	1.1180	1.1205	1.1261	1.1262
∞	1.0000	1.0000	1.0000	1.0000	1.0000	1.0000	1.0000	1.0000	1.0000
				F_z^s					
0.50	1.1646	1.1727	1.2118	1.3881	3.0294	3.5751	3.6749	3.7712	3.7900
0.55	1.1797	1.1926	1.2409	1.4740	2.5227	3.1772	3.3206	3.4327	3.4562
0.75	1.2121	1.2333	1.3078	1.6102	1.9860	2.3649	2.4648	2.5368	2.5511
1.00	1.2544	1.2789	1.3570	1.5055	1.6773	1.9052	1.9735	2.0226	2.0315
2.00	1.2693	1.2652	1.2733	1.2814	1.3159	1.3649	1.3871	1.4056	1.4080
5.00	1.1187	1.1176	1.1173	1.1171	1.1242	1.1240	1.1275	1.1345	1.1350
∞	1.0000	1.0000	1.0000	1.0000	1.0000	1.0000	1.0000	1.0000	1.0000

TABLE 2. Typical values of F_z^t and F_z^s for $\tilde{a} = 0.5$.

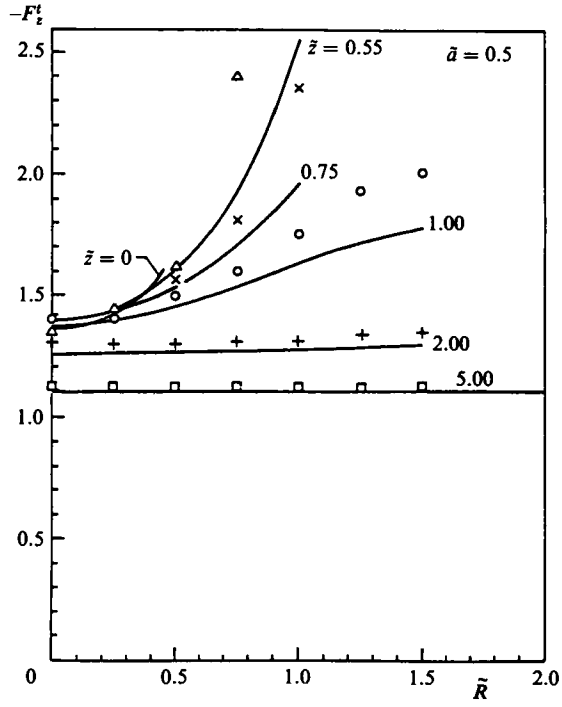

FIGURE 3. Typical values of F_z^t for $a/R_0 = 0.5$: ——, Yan *et al.* (1985). Present study: △, $\tilde{z} = 0.55$; ×, 0.75; ○, 1.00; +, 2.00; □, 5.00.

pore edge varies with angle ϕ. The axisymmetric values of F_z^t and F_z^s for a sphere of radius a near an orifice of radius ρ are averaged over ϕ and these average values are taken as our approximation. In cases (*b*) and (*c*), for some ranges of ϕ the sphere centre sees an infinite plane or a disk of finite size rather than a pore. Then the appropriate known solutions are used in the averaging process.

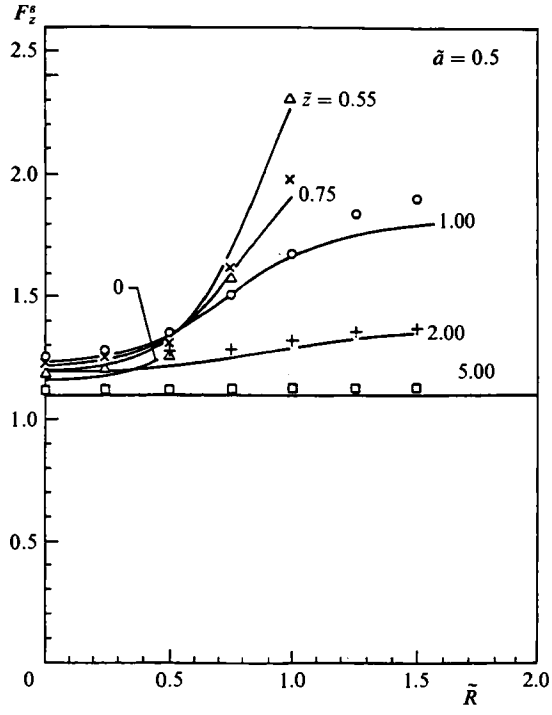

FIGURE 4. Typical values of F_z^s for $a/R_0 = 0.5$. Symbols as in figure 3.

Typical values of F_z^t and F_z^s as functions of particle position for $\tilde{a} = 0.5$ are given in table 2 and figures 3 and 4. Also shown in the figures are the recent numerical solutions of Yan *et al.* (1985). The reasonable agreement at virtually all locations confirms the plausibility of the interpolations used. Tables for all the force and torque coefficients using the foregoing approximations are given in Yan (1985). The numerical solution for the three-dimensional pore-entrance geometry in Yan *et al.* (1985) shows that, in accordance with assumptions (i) and (ii), F_z^r, $T_\phi^{t,z}$ and $T_\phi^{s,z}$ are an order of magnitude smaller than the other coefficients and that the radial dependence of the six coefficients listed under assumption (ii) is small.

Using the above assumptions, we can simplify (7) and (8) to

$$\left.\begin{aligned} U_R^0 &= -\frac{F_R^s - \frac{a}{2z} F_R^r T_\phi^{s,R}/T_\phi^r}{F_R^t - F_R^r T_\phi^{t,R}/T_\phi^r} V_R, \\ U_z^0 &= -\frac{F_z^s}{F_z^t} V_z, \end{aligned}\right\} \tag{34}$$

and

$$\left.\begin{aligned} D_{RR} &= D_\infty \left(\frac{-1}{F_R^t - F_R^r T_\phi^{t,R}/T_\phi^r}\right), \quad D_{Rz} = 0, \\ D_{zR} &= 0, \qquad\qquad\qquad\qquad D_{zz} = D_\infty \left(\frac{-1}{F_z^t}\right), \end{aligned}\right\} \tag{35}$$

Typical values of D_{RR}/D_∞ for $a/R_0 = 0.1$–1.5 are plotted in figure 5. If it were not for the hydrodynamic interaction of the particle with the entrance geometry, these

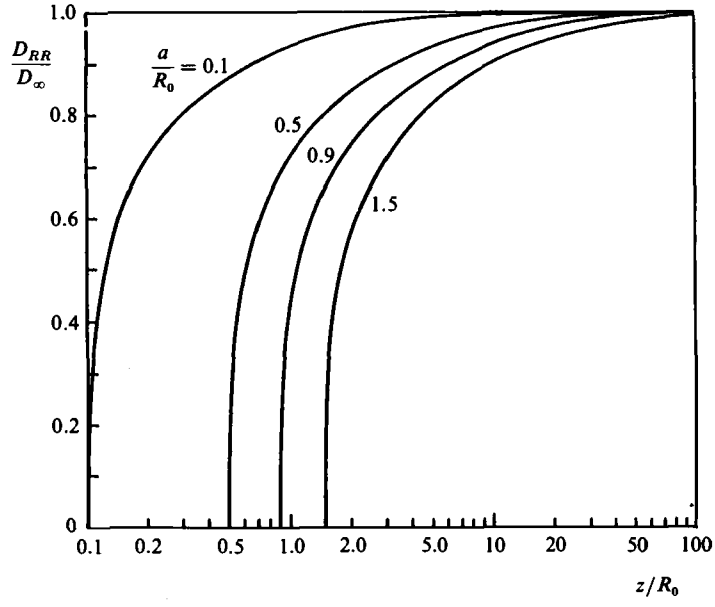

FIGURE 5. The diffusivity D_{RR}.

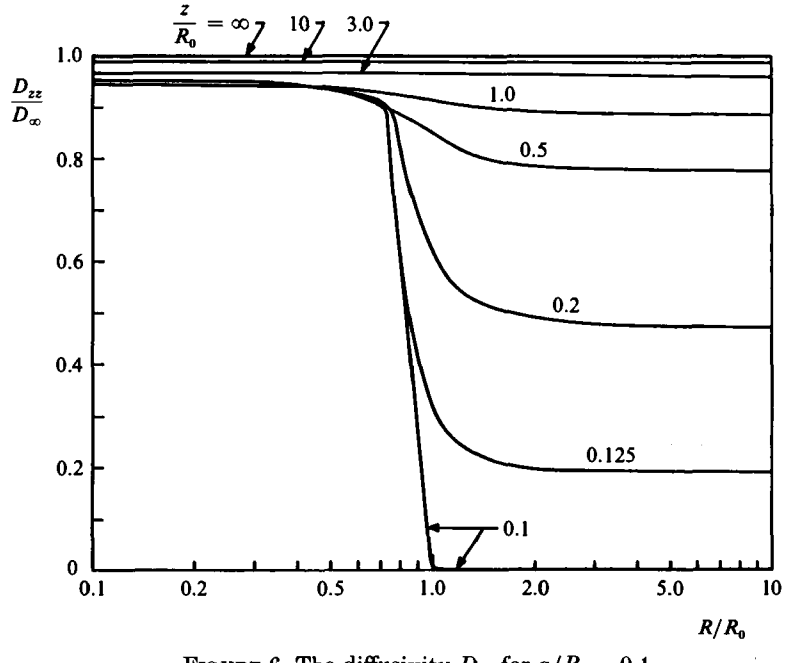

FIGURE 6. The diffusivity D_{zz} for $a/R_0 = 0.1$.

values would have been unity. The very rapid changes near $z = a$ and the slow approach to unity as z increases show the profound influence of the wall interaction. Because of our simplifying assumptions D_{RR} is independent of R.

Figure 6 gives the changes in D_{zz}/D_∞ with R/R_0 for $a/R_0 = 0.1$. When $z > R_0$, the dependence on R is very weak but, as the plane wall is approached, D_{zz} decays rapidly to zero.

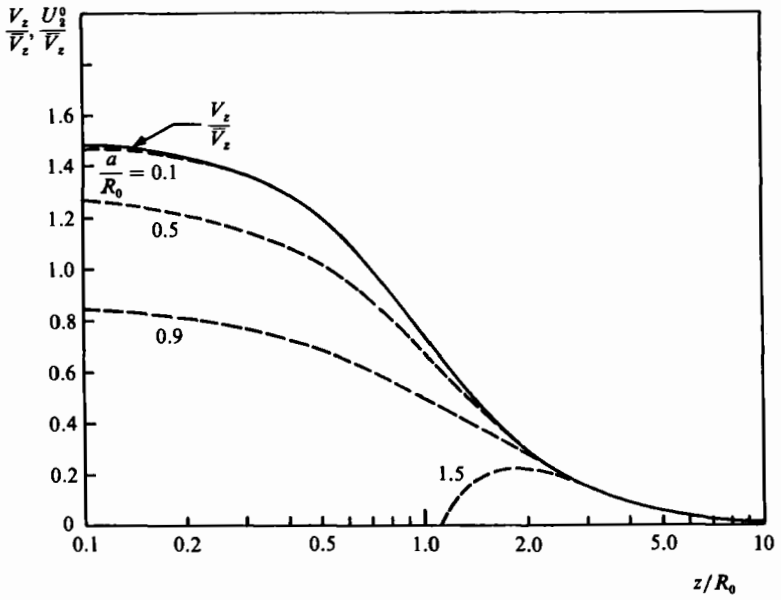

FIGURE 7. The particle's deterministic velocity U_z^0 and the solvent velocity V_z along the centreline: ——, $V_z/\overline{V}_z$; --- $U_z^0/\overline{V}_z$, $R = 0$.

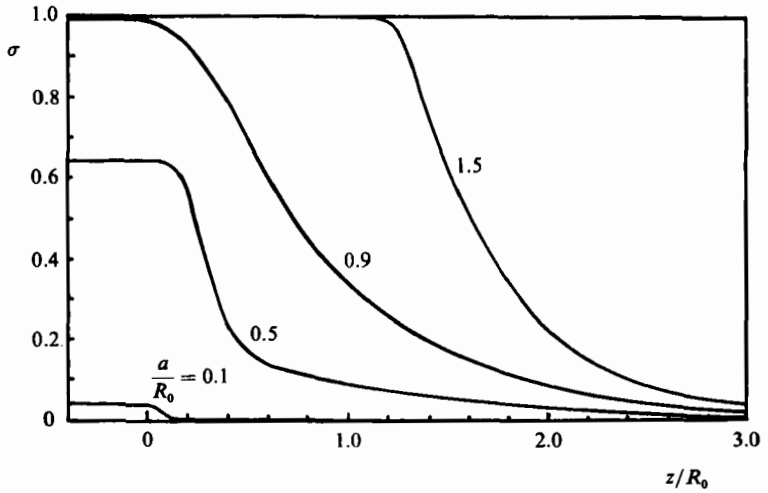

FIGURE 8. The local reflection coefficient σ along the centreline.

Figure 7 shows the ratios of the solvent velocity V_z and the deterministic velocity U_z^0 to the average velocity $\overline{V}_z$ in the pore for $a/R_0 = 0.1$–1.5. It is seen that a substantial slip velocity is generated between the two phases when the particle is close to the pore entrance for $a/R_0 > 0.5$.

Figure 8 presents some typical values for the local reflection coefficient $\sigma(z)$ along the pore axis ($R = 0$). It is seen that within a few particle radii $\sigma(z)$ changes from σ_0 (the value inside the pore) to almost zero.

3. Numerical procedures

In the solute-conservation equation (9), $\boldsymbol{U}^0$ is related to the osmotic flow rate q through (7) and (21a, b). However, (27) and (33) show that q depends not only on the concentration difference across the membrane, but also on the concentration profile and the local reflection coefficient in the entrance/exit regions. This makes the problem nonlinear. Since the concentration profile is not known in advance, one has to solve this problem by an iterative procedure. To start, an initial profile of concentration has to be guessed, which will then be used to calculate q from (27) or (33). With this q, the solvent velocity can be evaluated from (21a, b) and (16), and then $\boldsymbol{U}^0$ and $\boldsymbol{D}$ from (7), (8), (11) and (12). With these values, the solute-conservation equation (20a) will be solved subject to boundary conditions (20b)–(20f) (for a permeable membrane) or (28a)–(28c) (for a semi-permeable membrane) in the right half-space. For a permeable membrane (20a) should also be solved in the left half-space subject to equivalent conditions to (20b)–(20f). The concentration profile so obtained may be used to recalculate q from (27) or (33). The above procedures are then repeated until the concentration profile is determined to within the required accuracy. Finally one can find the pressure profile from (23), (18), (25), (30) or (31).

Quantities are non-dimensionized in terms of R_0, C_∞, D_∞ and μ such that

$$\tilde{C} = \frac{C}{C_\infty}, \quad \tilde{p} = \frac{pR_0^2}{\mu D_\infty}, \quad \tilde{q} = \frac{q}{\pi R_0 D_\infty}, \tag{36}$$

where D_∞ is given by (8a). Dimensional analysis shows that the osmotic flow just described is governed by three dimensionless parameters, i.e. two dimensionless lengthscales $\tilde{a} = a/R_0$ and $\tilde{l} = l/R_0$ and a dimensionless group

$$N_q = \frac{9}{2\pi}\frac{\phi}{\tilde{a}^2}, \tag{37}$$

where

$$\phi = \tfrac{4}{3}\pi a^2 N_A C_\infty \tag{38}$$

is the volume fraction of the solute in the right bulk solution. N_q describes the strength of the osmosis, as can be seen from the dimensionless forms of (27) and (33):

$$\tilde{q} = \frac{N_q}{3+\frac{8}{\pi}\tilde{l}}\left[\sigma_0(\tilde{C}_0 - \tilde{C}_l) + \int_0^\infty \sigma(\tilde{z})\frac{\partial \tilde{C}}{\partial \tilde{z}}\,\mathrm{d}\tilde{z} - \int_{-\tilde{l}}^{-\infty} \sigma(\tilde{z})\frac{\partial \tilde{C}}{\partial \tilde{z}}\,\mathrm{d}\tilde{z}\right],$$

(for a permeable membrane), (39)

$$\tilde{q} = \frac{N_q}{3+\frac{8}{\pi}\tilde{l}}\left[\tilde{C}(\tilde{z}_a^+) + \int_0^\infty \sigma(\tilde{z})\frac{\partial \tilde{C}}{\partial \tilde{z}}\,\mathrm{d}\tilde{z}\right] \quad \text{(for a semi-permeable membrane).} \tag{40}$$

Numerical calculations have been performed for a wide range of particle sizes $0.01 < \tilde{a} < 1.5$ and pore lengths $5 < \tilde{l} < 500$. In all the cases ϕ has been limited to a maximum value of 0.05 so that the solution can be treated as dilute. The corresponding N_q ranges between 716.2 and 0.006. Without loss of generality, we assume $C_{-\infty} = 0$, since one can always use the scale transformation

$$\hat{C} = \frac{C - C_{-\infty}}{C_\infty - C_{-\infty}}$$

to convert a non-zero concentration $C_{-\infty}$ to this case.

In our calculations, (20) is discretized into the form of a difference equation in a

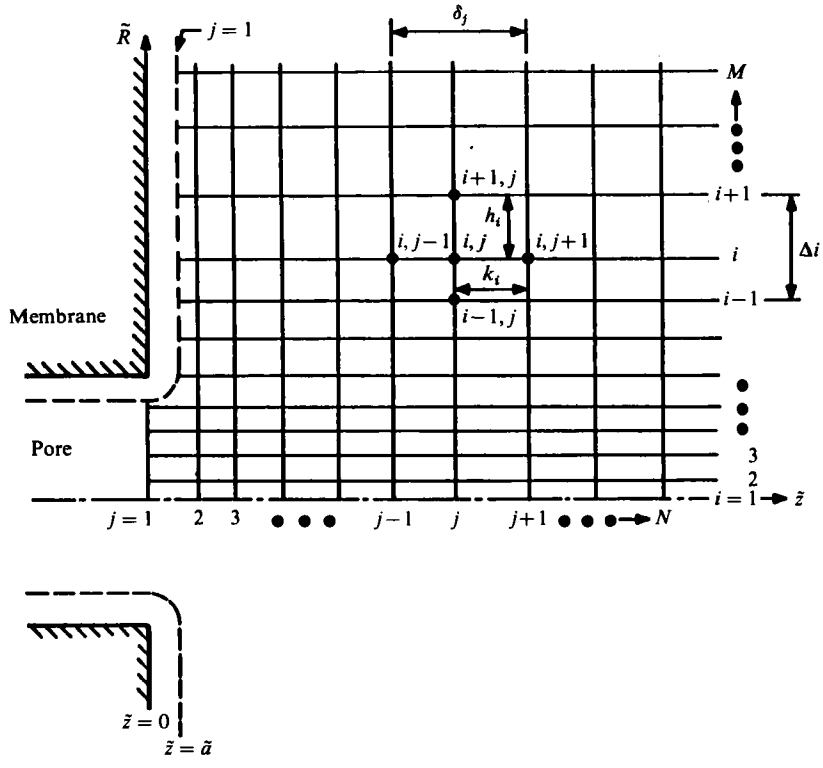

FIGURE 9. The grid system for solving equation (20).

grid system as shown in figure 9 (for the case of a permeable membrane), where the infinite right half-space is truncated to a big finite region and the broken curve constitutes part of the boundary. The spacings in figure 9 are unevenly arranged so that the finer grids near the pore opening may better describe the rapid concentration change there. The detailed discretization can be found in Yan (1985). The resulting difference equation is then solved by using the over-relaxation scheme (Forsythe & Wasow 1960). The choice of the relaxation factor can influence the convergence speed significantly. Numerical tests indicated that the optimum values of this factor fell between 1.5 and 1.9. The convergence was tested by requiring that, in the iterative process, the two successive values of the concentration at every point should differ from each other by less than a given small positive number ϵ. It was found that $\epsilon = 10^{-6}$ was a good choice and $\epsilon = 10^{-5}$ may occasionally lead to false convergence. For most cases sixty to a few hundred iterations are sufficient.

4. Results and discussion

Representative solutions for the axial pressure and concentration profiles for small particles in a long and a short pore are shown in figures 10 and 11 respectively. For the long pore the entrance and exit effects are minor and both the pressure and concentration changes are confined to the membrane interior. The flow follows a Poiseuille pressure drop over most of the pore length that is established by a steep concentration gradient near the pore exit. The high osmotic flow causes the solute to be swept to the downstream end of the pore, but there is little exit correction outside the membrane since the hydrodynamic interaction in this region is an

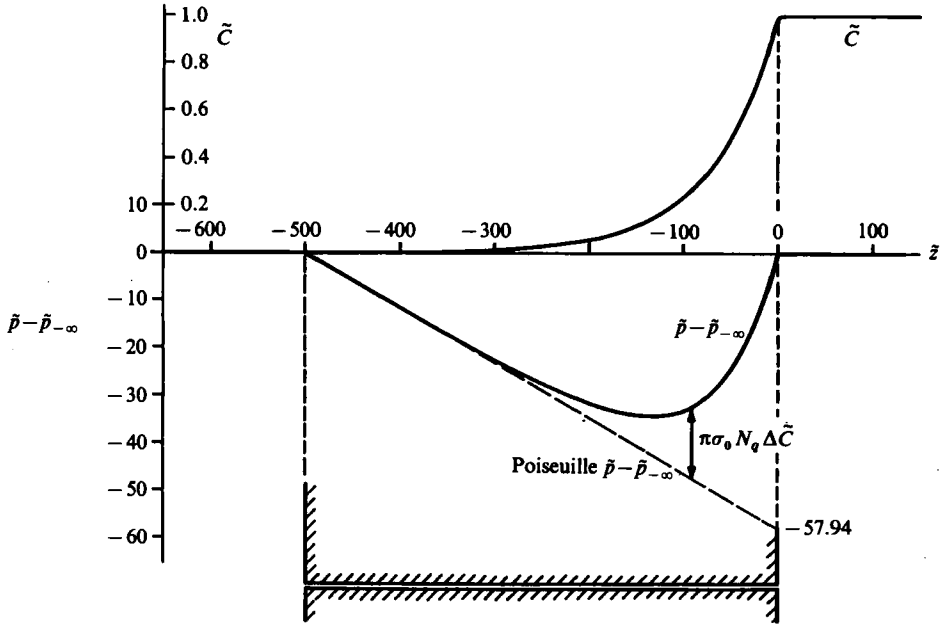

FIGURE 10. The concentration and pressure profiles for $\tilde{a} = 0.01$, $\phi = 0.05$, $\tilde{l} = 500$, $N_q = 716.2$, $\tilde{q} = 0.01447$.

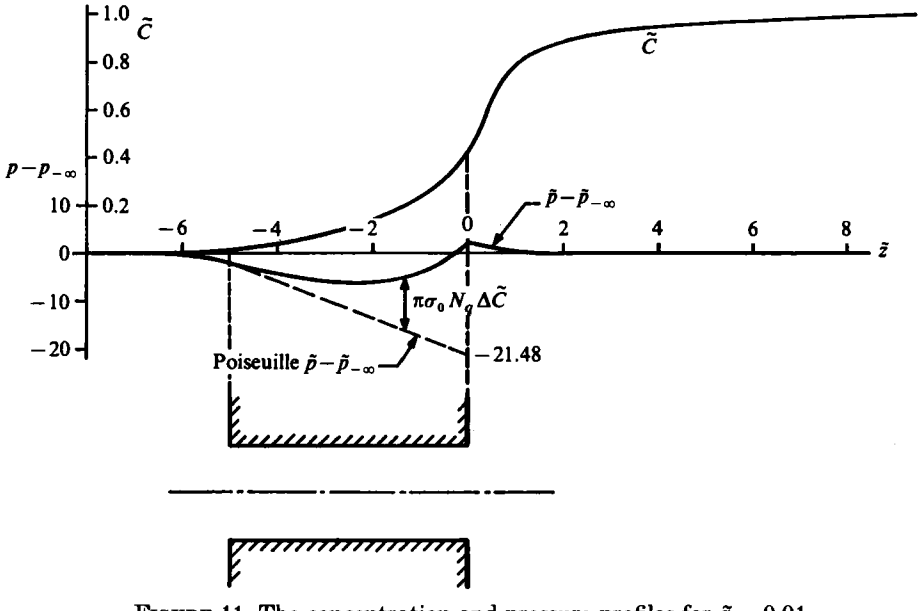

FIGURE 11. The concentration and pressure profiles for $\tilde{a} = 0.01$, $\phi = 0.05$, $\tilde{l} = 5$, $N_q = 716.2$, $\tilde{q} = 0.4807$.

insignificant fraction of the total resistance. In contrast, for the short pore shown in figure 11 a very significant fraction of the total concentration drop occurs in the outer bathing solution and the pressure profile bears little resemblance to the Poiseuille distribution. The large asymmetry between the pore entrance and exit regions, which is contrary to Lerche's (1976) hypothesis, is caused by convection. There is an

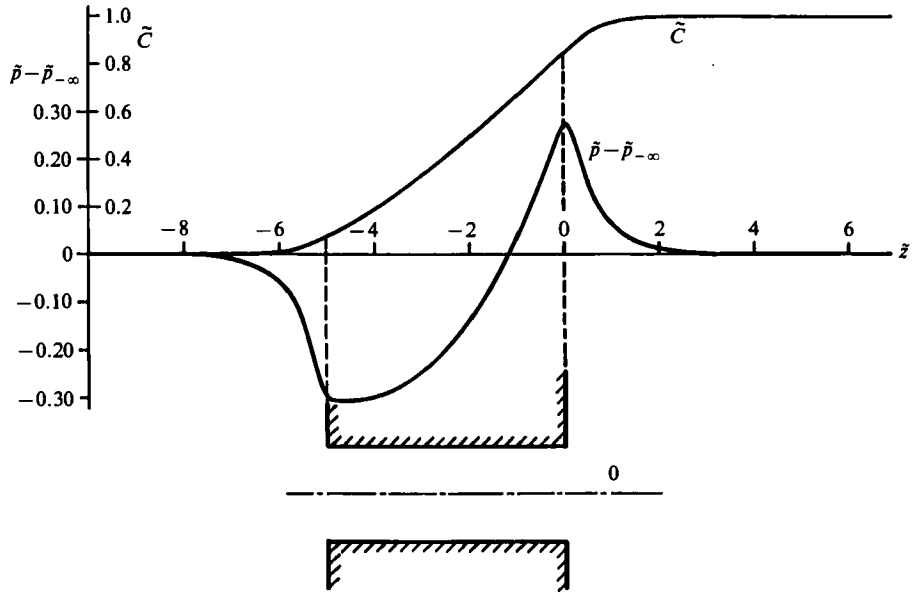

FIGURE 12. The concentration and pressure profiles for $\tilde{a} = 0.1$, $\phi = 0.05$, $\tilde{l} = 5$, $N_q = 7.162$, $\tilde{q} = 0.07022$.

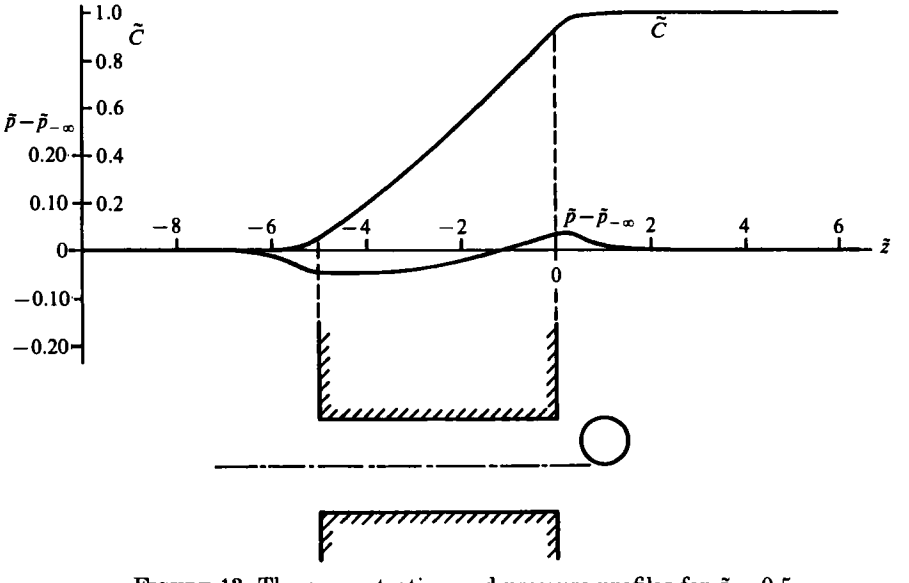

FIGURE 13. The concentration and pressure profiles for $\tilde{a} = 0.5$, $\phi = 0.05$, $\tilde{l} = 5$, $N_q = 0.286$; $\tilde{q} = 0.01365$.

interesting maximum in the pressure profile at the exit plane. For both the long and short pores there are substantial regions where the solvent is moving against an adverse pressure gradient due to the presence of local osmotic forces. This effect is more dramatically shown in figure 12 for $\tilde{a} = 0.1$ and $\tilde{l} = 5$, where the solvent moves against an adverse pressure gradient over the entire pore length.

Figures 13 and 14 show the pressure and concentration profiles for medium-sized

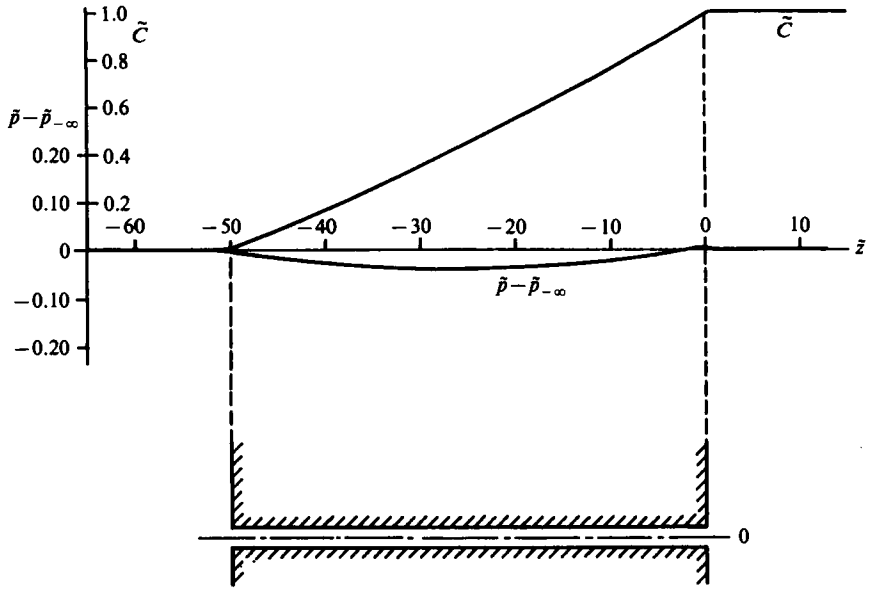

FIGURE 14. The concentration and pressure profiles for $\tilde{a} = 0.5$, $\phi = 0.05$, $\tilde{l} = 50$, $N_q = 0.286$, $\tilde{q} = 0.00172$.

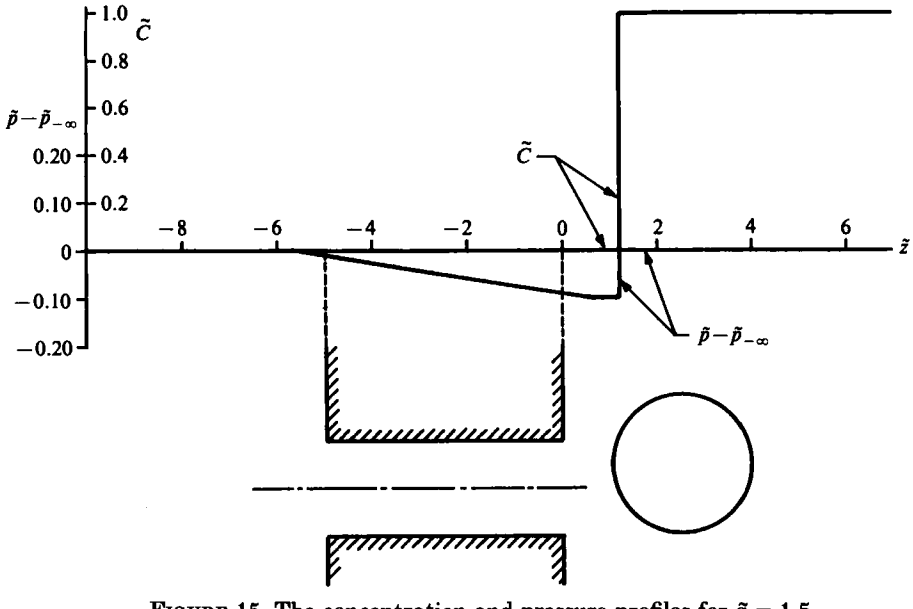

FIGURE 15. The concentration and pressure profiles for $\tilde{a} = 1.5$, $\phi = 0.05$, $\tilde{l} = 5$, $N_q = 0.032$, $\tilde{q} = 0.00203$.

particles in a short and a relatively long pore respectively. Since the strength of the osmotic flow is inversely proportional to $\tilde{a}^2$ when the volume fraction ϕ of the solute in the bulk solution is fixed (see 37)), small osmotic flow rates are obtained by a low concentration of large particles even though these particles have a large reflection coefficient. Note that the scale for the pressure drop in these figures is two orders of magnitude smaller than in figures 10 and 11. The maximum pressure drops in these

$\tilde{l}$	$\tilde{a}$	N_q	$\tilde{q}$	q_0/q	L_{p0}/L_p	$\tilde{C}_0$	$\tilde{C}_l$
5	0.01	716.2	4.807×10^{-1}	3.089	1.236	0.408	0.013
	0.1	7.162	7.022×10^{-1}	1.563	1.236	0.838	0.069
	0.5	0.286	1.365×10^{-2}	1.294	1.236	0.924	0.047
	0.9	0.088	5.426×10^{-3}	1.267	1.236	0.866	0.051
	1.5	0.032	2.034×10^{-3}	1.236	1.236	0	0
50	0.01	716.2	1.184×10^{-1}	1.254	1.024	0.814	0
	0.1	7.162	1.043×10^{-2}	1.052	1.024	0.978	0.008
	0.5	0.286	1.719×10^{-3}	1.027	1.024	0.991	0.001
	0.9	0.088	6.723×10^{-4}	1.025	1.024	0.986	0.005
	1.5	0.032	2.455×10^{-4}	1.024	1.024	0	0

TABLE 3. Osmotic flux for $\phi = 0.05$

$\tilde{l}$	$\tilde{a}$	ϕ	$\tilde{q}$	q_0/q	L_{p0}/L_p	$\tilde{C}_0$	$\tilde{C}_l$
5	0.01	4×10^{-7}	7.191×10^{-6}	1.730	1.236	0.872	0.128
	0.1	4×10^{-4}	5.905×10^{-4}	1.479	1.236	0.905	0.094
	0.3	0.0108	5.409×10^{-3}	1.347	1.236	0.930	0.063
	0.5	0.0500	1.365×10^{-2}	1.294	1.236	0.924	0.047
50	0.01	4×10^{-7}	1.124×10^{-6}	1.107	1.024	0.983	0.017
	0.1	4×10^{-4}	8.405×10^{-5}	1.039	1.024	0.989	0.011
	0.3	0.0108	7.047×10^{-4}	1.034	1.024	0.992	0.007
	0.5	0.0500	1.719×10^{-3}	1.027	1.024	0.991	0.001

TABLE 4. Osmotic flux for $C_\infty = 2.477\times10^{-6}$ mol/cm^3 and $R_0 = 4$ nm

figures are about one-tenth of the Poiseuille pressure drop $8\tilde{q}\tilde{l}$ along the whole pore length and there is no longer the sweeping-away effect of the solute near the exit end.

Figure 15 illustrates the osmotic behaviour for a semi-permeable membrane. The steric exclusion of particles of radius $a > R_0$ produces an interface with a discontinuity in both concentration and pressure. To the left of this interface the concentration is identically zero and to the right the concentration is essentially uniform. The osmotic flow is so weak that the convection at the pore exit has only a very minor effect on the concentration profile.

The entrance/exit effects for different particle sizes, pore lengths and N_q are summarized in table 3 (for a constant volume fraction ϕ) and table 4 (for a constant molar concentration C_∞ and a given pore radius R_0). The results for the osmotic flux q are obtained from (39) or (40) and q_0 is the flux that would be obtained if the entrance/exit effects were neglected. The ratio of the hydraulic permeabilities without and with the entrance/exit effects are calculated from the following:

$$\frac{L_{p0}}{L_p} = 1 + \frac{3\pi}{8\tilde{l}}. \tag{41}$$

It is evident from the tables that for small particles the entrance/exit effects are more significant for the osmotic flux than for the hydraulic permeability, because of the additional changes due to the concentration profiles. If the entrance/exit effects were not taken into consideration, the osmotic flow rate of the solvent may be overestimated by as much as 200 % for very small particles in a short pore (e.g. $\tilde{a} = 0.01$ and $\tilde{l} = 5$),

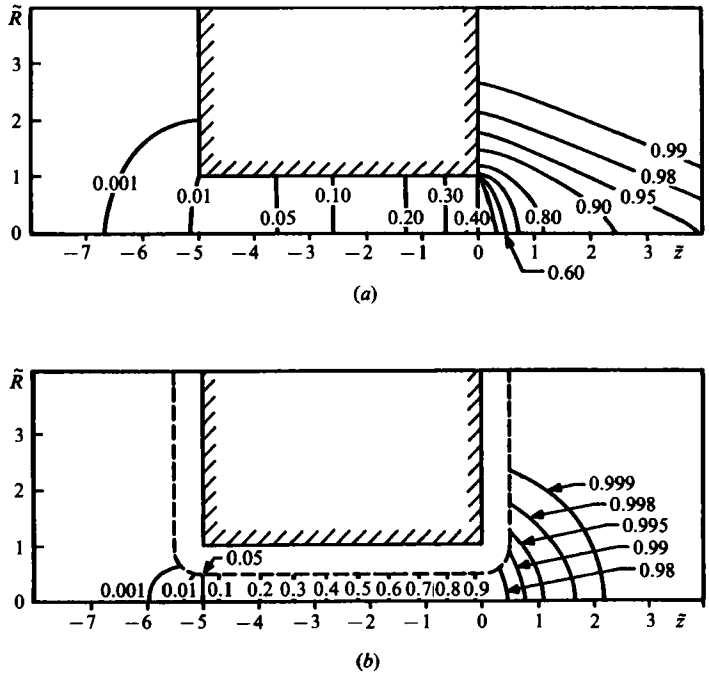

FIGURE 16. The isoconcentration curves: (*a*) $\tilde{a} = 0.01$, $\phi = -0.05$, $\tilde{l} = 5$; $N_q = 716.2$, $\tilde{q} = 0.4807$; (*b*) $\tilde{a} = 0.5$, $\phi = 0.05$, $\tilde{l} = 5$, $N_q = 0.286$, $\tilde{q} = 0.01365$.

although these effects are insignificant for the reflection coefficient. The smaller the solute particle, the shorter the pore, and, the higher the volume fraction ϕ, the more important are the entrance/exit effects. Even with a relatively long pore ($\tilde{l} = 50$) and a very low volume fraction ($\phi = 4 \times 10^{-7}$), the entrance/exit effects may still influence the osmotic flux by more than 10% for very small particles ($\tilde{a} = 0.01$). On first thought it may seem paradoxical that large changes in osmotic flux can be caused by particles with a small reflection coefficient. However, inspection of (39) and (40) shows that in the entrance and exit regions it is the product of σ and the local concentration gradient in these regions which is important and not σ alone.

In figure 16 the isoconcentration lines are plotted for two different particle sizes. While the concentration change occurs mainly inside the pore for $\tilde{a} = 0.5$, the greatest gradient of concentration occurs immediately outside the pore entrance for $\tilde{a} = 0.01$. However, in both cases the entrance/exit effects are essentially confined to the regions within a few pore radii from the pore openings.

Figure 16 clearly demonstrates the three-dimensional, local nature of the entrance/exit effects. For most biological membranes, the porosity η is very low and the pore radius is small compared with the pore spacing. Therefore, the above local concentration changes would occur in the vicinity of the pore entrance/exit and not be affected by the interaction between pores. As schematically shown in figure 17, the flows through different pores become well mixed at a distance δ_1 from the exit plane of the membrane and a quasi-uniform concentration C_w is achieved. This length δ_1 is characteristic of the pore spacing. Only beyond this δ_1 can the flow be treated as one-dimensional and Pedley's model for the unstirred layer applied, where C_w serves as the effective membrane concentration C_m. At low porosities (e.g. $\eta = 0.01$),

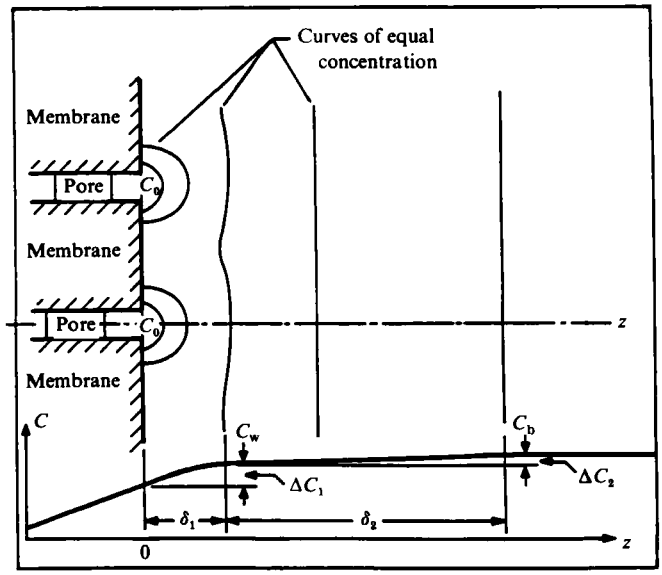

FIGURE 17. Two lengthscales in the entrance region and the unstirred layer.

the axial velocity of this one-dimensional flow would be much lower than the average velocity V_z inside the pore (by a factor η). Hence, it can be expected that the change beyond δ_1 would be much weaker and on a much longer lengthscale, say δ_2, than that within δ_1. In fact, as Pedley & Fischbarg (1978) estimated, based on the experimental data of Lerche (1976), δ_2 is about 500 μm and $C_b - C_w = \Delta C_2$ in this region is less than 2% of the bulk concentration C_b for most biological membranes. Our results show that the concentration gradient $\Delta C_1/\delta_1$ within the entrance/exit region of fine lengthscale δ_1 may be several orders of magnitude greater than the concentration gradient $\Delta C_2/\delta_2$ in Pedley's unstirred layer of lengthscale δ_2 for the case of a permeable membrane.

The foregoing discussion and the results in figure 16 provide a much clearer picture of the substructure of the unstirred layer described by Dainty, Pedley and others. When the porosity is low the concentration C_w acts as the far-field solution C_∞ for the isolated pore in figure 1 (*a*) since the concentration relaxes to this value in both the R- and z-directions within a few pore radii. However, if the pores are closely spaced (less than about three pore radii), the far-field boundary conditions C_w or C_∞ on the inner lengthscale δ_1 cannot be applied for an isolated pore, but the interaction between pores must be considered. In this case the concentration in the exit plane of the membrane will not relax to C_w as R increases, and an intermediate layer relating the wall concentration and Pedley's C_m must be considered. For finite non-isotonic bathing solutions ($C_\infty \neq C_{-\infty}$), there would be a solute flow towards the dilute side and consequently C_∞ and $C_{-\infty}$ would change with time. A steady state could not be reached until $C_\infty = C_{-\infty}$. Lerche (1976) claimed that curve 3 (at $t = 121$ s) in his figure 4 was a steady state, but curve 5 (at $t = 576$ s) and curve 6 (at $t = 900$ s) in the same figure show an obvious continuing change. However, at any instant a quasi-steady-state solution does exist within the fine scale δ_1 once the instantaneous value of C_w, as shown in figure 17, is used for our C_∞ in figure 1 (*a*). This means that, corresponding to the two different lengthscales δ_1 and δ_2, there are also two different timescales, one for the local changes within δ_1 (fast) and one for the long-scale changes

within δ_2 (slow). A combined time-dependent analysis of both the layers would be interesting.

In summary, our model has quantitatively described the pore entrance/exit effects on osmosis for both permeable and semi-permeable membranes. It is found that for a permeable membrane there are fine-scale entrance/exit regions where the three-dimensional concentration changes are much greater than in the much thicker one-dimensional unstirred layer. The neglect of these effects may result in significant errors in estimating the osmotic flux for small particles and short pores although the reflection coefficient itself may be quite small.

The present model is greatly simplified in geometry and applies to dilute solutions only. For non-dilute solutions, the expressions for the osmotic pressure and the thermodynamic force have to be modified and the hydrodynamic interactions between the solute particles cannot be neglected. Moreover, the solvent velocity V can no longer be approximated by that in the absence of particles as is done herein.

The authors wish to thank the National Science Foundation for supporting this research under grant ENG82-00301 and The City University of New York Computer Center for the use of their facilities. The helpful discussions with Professors R. Skalak, A. Silberberg and P. Ganatos are appreciated. This work has been performed in partial fulfilment of the requirements for the Ph.D. degree of Z. Yan from the School of Engineering of The City College of The City University of New York.

REFERENCES

ANDERSON, J. L. 1981 *J. Theor. Biol.* **90**, 405.

ANDERSON, J. L. & ADAMSKI, R. P. 1983 *AIChE Symp. Series* **222**, 79.

ANDERSON, J. L. & MALONE, D. M. 1974 *Biophys. J.* **14**, 957.

ANDERSON, J. L. & QUINN, J. A. 1974 *Biophys. J.* **14**, 130.

BATCHELOR, G. K. 1976 *J. Fluid Mech.* **74**, 1.

BRENNER, H. 1961 *Chem. Engng Sci.* **16**, 242.

BRENNER, H. & GAYDOS, L. J. 1977 *J. Colloid Interface Sci.* **58**, 312.

COX, R. G. & BRENNER, H. 1967 *Chem. Engng Sci.* **22**, 1753.

DAGAN, Z., PFEFFER, R. & WEINBAUM, S. 1982 *J. Fluid Mech.* **122**, 273.

DAGAN, Z., WEINBAUM, S. & PFEFFER, R. 1982*a* *J. Fluid Mech.* **115**, 505.

DAGAN, Z., WEINBAUM, S. & PFEFFER, R. 1982*b* *J. Fluid Mech.* **117**, 143.

DAINTY, J. 1963 *Adv. Bot. Res.* **1**, 279.

FORSYTHE, G. E. & WASOV, W. R. 1960 *Finite-Difference Methods for Partial Differential Equations.* Wiley.

GANATOS, P., WEINBAUM, S., FISCHBARG, J. & LIEBOVITCH, L. 1980 *Adv. in Bioengng*, p. 193. ASME.

GOLDMAN, A. J., COX, R. G. & BRENNER, H. 1967 *Chem. Engng Sc.* **22**, 637.

HAPPEL, J. & BRENNER, H. 1973 *Low Reynolds Number Hydrodynamics*, 2nd edn. Noordorff.

HSIEH, J. S. 1975 *Principles of Thermodynamics.* McGraw-Hill.

KEDEM, O. & KATCHALSKY, A. 1958 *Biochem. Biophys. Acta* **27**, 229.

LEICHTBERG, S., PFEFFER, R. & WEINBAUM, S. 1976 *Intl J. Multiphase Flow* **3**, 147.

LERCHE, D. 1976 *J. Membrane Biol.* **27**, 193.

LEVITT, D. G. 1975 *Biophys. J.* **15**, 533.

MAURO, A. 1957 *Science* **126**, 252.

PEDLEY, T. J. & FISCHBARG, J. 1978 *J. Theoret. Biol.* **70**, 427.

PEDLEY, T. J. 1980 *J. Fluid Mech.* **101**, 843.

PEDLEY, T. J. 1981 *J. Fluid Mech.* **107**, 281.

RAY, P. M. 1960 *Plant Physiol.* **35**, 783.

YAN, Z. Y. 1985 Three Dimensional Hydrodynamic and Osmotic Pore Entrance Phenomena. Ph.D. dissertation. The City University of New York.

YAN, Z. Y., WEINBAUM, S., GANATOS, P. & PFEFFER, R. 1985 The three-dimensional hydrodynamic interaction of a finite sphere with a circular orifice at low Reynolds number. Submitted to *J. Fluid Mech.*